Journal of Hazardous Materials 172 (2009) 1229–1235

Contents lists available at ScienceDirect

Journal of Hazardous Materials

journal homepage: www.elsevier.com/locate/jhazmat

Oxidative and antibacterial activity of Mn_3O_4

Al-Nakib Chowdhury*, Md. Shafiul Azam*, Md. Aktaruzzaman, Abdur Rahim

Department of Chemistry, Bangladesh University of Engineering and Technology, Dhaka-1000, Bangladesh

ARTICLE INFO

Article history:
Received 11 June 2009
Received in revised form 23 July 2009
Accepted 29 July 2009
Available online 5 August 2009

Keywords:
Nanoparticles
Mn_3O_4
Dye degradation
Antibacterial activity
Polyaniline

ABSTRACT

Mn_3O_4 nanoparticles with diameter *ca.* 10 nm were synthesized by the forced hydrolysis of Mn(II) acetate at 80 °C. The X-ray diffraction (XRD), Fourier transform infra red (FT-IR) spectroscopy, scanning electron microscopy (SEM) and energy dispersive X-ray (EDX) techniques were employed to study structural features and chemical composition of the nanoparticles. The unique oxidative activity of the Mn_3O_4 nanoparticles was demonstrated in the polymerization and dye degradation reactions. On adding Mn_3O_4 suspension to an acidic solution of aniline, yielded immediately green sediment of polyaniline (PANI). The organic dyes, *viz*., methylene blue (MB) and procion red (PR) were found to be completely decolorized from their aqueous solution on treating the dyes with Mn_3O_4 suspension in acidic media. The Mn_3O_4 nanoparticles also showed a clear antibacterial activity against the *Vibrio cholerae*, *Shigella sp*., *Salmonella sp*., and *Escherichi coli* bacteria that cause cholera, dysentery, typhoid, and diarrhea diseases, respectively.

1. Introduction

Mn_3O_4 nanoscale materials have stimulated a great interest due to their special electronic and structural features with unique ion-exchange, molecular adsorption, catalysis, electrochemical, and magnetic properties [1–3]. It has been reported that Mn_3O_4 is a promising electrochromic material of anodic coloration since it has a reversible color change from brown (colored state) to yellow (bleached state) [4]. Mn_3O_4 is also known to be an active catalyst in several oxidations or reductions, for example, it can be used as catalyst for the oxidation of methane and carbon monoxide [5] or the selective reduction of nitrobenzene [6]. Moreover, Mn_3O_4 with different polymorphs has been found to be an active and stable catalyst for the combustion of organic compounds in the temperature range of 373–773 K [7]. These combustion-related catalytic technologies are of interest in relation to several air-pollution problems, allowing limitation of the emission of NO*x* and volatile organic compounds from waste gases of different origins [8].

Manganese oxides are also powerful oxidants due to their high reducing potential. It has already been reported that Mn^{3+} and Mn^{4+} oxides and hydroxides can oxidize many inorganic compounds including Co(II), Cr(III), As(III), Sb(III) and Se(IV) [9–13] and also a variety of natural and xenobiotic organic compounds such as catechol, quinines, substituted phenols, aromatic amines, pesticides, and explosives (e.g. TNT) [14–18]. Mn_3O_4 (hausmannite) is a complex oxide of Mn containing both di- and tri-valent manganese. Redox potential and pH have been used extensively to evaluate equilibrium relationships between Mn(II) activity in solution and various Mn compounds. Reducing potential of Mn_3O_4 is higher than that of the other Mn oxides [19]. Table 1 shows the reducing potentials of some manganese oxides.

Growing concern for public health and environmental quality has prompted a special interest in developing and implementing various materials and methods for removing the toxic organic and inorganic pollutants from water. Dyes from the effluent of textile industries are the major sources of water contamination [20]. Apart from the aesthetic desirability of colored streams resulting from dye waste, the presence of dyes in water reduces light penetration and hinders photosynthesis in aquatic plants [21]. Some dyes and their degradation products in surface water are reported to be highly carcinogenic [22]. It is, therefore, essential to treat the dye effluents prior to their discharge into the receiving water.

For pollution remediation purposes, land-born natural Mn ores, synthetic nascent state Mn oxides and materials coated/modified with Mn oxides have been tested as scavenger for removal of Pb^{2+}, Cd^{2+}, Cu^{2+}, 17 α-ethynylestradiol [23–26], as oxidant for degradation of organic pollutants [27,28] and as oxidant and/or adsorbent for removal of As(III) and As(V) [29].

In view of strong oxidative and other unique characteristics of the Mn_3O_4, it seems to be interesting to evaluate possible application of Mn_3O_4 as an effective oxidant for the polymerization of aniline and degradation of organic contaminants in water. In this study, decolorization of methylene blue (MB), procion red (PR) and a dye contaminated real sample (dye effluent of a local textile industry) as the model organic contaminants was investigated using Mn_3O_4 as an oxidant. Bactericidal nanomaterials, particularly metallic nanoparticles, opened a new avenue in med-

* Corresponding authors. Tel.: +880 2 9665614; fax: +880 2 8613046.
E-mail addresses: nakib@chem.buet.ac.bd (A.-N. Chowdhury), azam@ualberta.ca, mdshafiulazam@chem.buet.ac.bd (Md.S. Azam).

0304-3894/$ – see front matter.
doi:10.1016/j.jhazmat.2009.07.129

Table 1
Standard reducing potential for some Mn oxides.

Redox couple	Redox reaction	Reducing potential (V)
MnO_2/Mn^{2+}	$MnO_2\ (s) + 4H^+ + 2e^- = Mn^{2+}\ (aq) + 2H_2O$	1.225
Mn_2O_3/Mn^{2+}	$Mn_2O_3\ (s) + 6H^+ + 2e^- = 2Mn^{2+}\ (aq) + 3H_2O$	1.497
Mn_3O_4/Mn^{2+}	$Mn_3O_4\ (s) + 8H^+ + 2e^- = 3Mn^{2+}\ (aq) + 4H_2O$	1.824

ical science. The bactericidal effect of silver nanoparticles on the micro-organisms is very well known. In the present study, antibacterial effect of Mn_3O_4 was also tested.

2. Experimental

2.1. Materials and reagents

Material and reagents include Mn(II) acetate [$Mn(OOCCH_3)_2.4H_2O$] (Merck, India), MB (E. Merck, Germany), PR (E. Merck, Germany), dye contaminated real sample (Young One, DEPZ, Bangladesh), sulphuric acid [H_2SO_4] (Merck, India), ammonium peroxidisulphate [$(NH_4)_2S_2O_8$] (Merck, India), N-methyl-2-pyrrolidone (NMP) (E. Merck, Germany), aniline (Merck, India), *Vibrio cholerae*, *Shigella sp*., *Salmonella sp*., and *Escherichi coli* bacteria (ICDDR,B, Bangladesh) and doubly distilled de-ionized water. All the chemicals and the reagents were of analytical grade and thus used without further purification except for aniline which was distilled twice under nitrogen atmosphere prior to its use.

2.2. Instruments

The surface morphology was examined by scanning electron microscopy (Philips XL30, Netherlands). Elemental contents were evidenced by energy dispersive X-ray (EDX) spectroscopy (Philips XL30, Netherlands). The crystallite size, structure and composition of the Mn_3O_4 were obtained by X-ray powder diffraction (XRD) method using a diffractometer (Philips, Expert Pro, Netherlands) with a Cu Kα radiation source ($\lambda = 1.5406$ Å) operated at 40 kV and 30 mA. FT-IR spectra were taken on a spectrometer (IR-470, Shimadzu, Japan) in the range 4000–400 cm^{-1}. Samples were thoroughly mixed and grinded with KBr powder to make a pellet for the FT-IR measurements. The electrochemical measurements were carried out with a potentiostat/galvanostat (Hokuto Denko, HABF 501, Japan) equipped with an X-Y recorder (Riken Denshi Co, Ltd., Japan). A UV–visible spectrophotometer (UV-1601 PC, Shimadzu, Japan) was employed to monitor degradation of dyes spectroscopically.

2.3. Experimental procedure and method of analysis

Mn_3O_4 nanoparticles were prepared by forced hydrolysis of Mn(II) acetate following the procedure reported previously [30]. In brief, the procedure is as follows: freshly prepared 0.4 M aqueous solution of $Mn(OOCCH_3)_2{\cdot}4H_2O$ was heated in an oven at 80 °C for 2 h. The resulting brown dispersed product, Mn_3O_4, was then quenched in cool water and recovered by centrifugation. The product was then washed several times with double distilled water and dried in air in an oven at 40 °C. For experiments, this Mn_3O_4 either as powder or its suspension was used. To make the suspension, desired amount of nanoparticles were just dispersed in the medium by gentle stirring.

Decolorization experiment was conducted in a glass beaker, typically containing 50 mL of 30 μM MB dye solution and 10 mL of 2.5 M H_2SO_4 yielding the solution pH 3. Then 50 mL aqueous suspension of Mn_3O_4 nanoparticles (0.25 g L^{-1}) was added to the dye solution. The mixture was kept undisturbed and allowed to react at room temperature. The progress of decolorization was assessed by spectroscopic measurements of the mixture at different time intervals (1 min to 24 h). To investigate the effect of pH on the decolorization process, experiment was also performed at pH 5 keeping the amount of Mn_3O_4 and the dye constant. Decolorization of PR dye was studied also in the same way by mixing 50 mL of 300 μM PR dye solution and 20 mL of 2.5 M H_2SO_4 to the suspension of 100 mL Mn_3O_4 nanoparticles (0.25 g L^{-1}) whereas for the real sample, 100 mL of the dye effluent and 2 mL of 2.5 M H_2SO_4 was mixed with 10 mL suspension of Mn_3O_4 nanoparticles (0.25 g L^{-1}).

Polyaniline (PANI) was prepared by the chemical oxidative polymerization of aniline with Mn_3O_4 nanoparticles as oxidant in an aqueous solution. In brief, 200 mL of aqueous solution was prepared by dissolving 1 mL of distilled aniline and 5.0 mL of 2.5 M H_2SO_4 and then 100 mL suspension of Mn_3O_4 nanoparticles (0.25 g L^{-1}) was added. After adding Mn_3O_4 nanoparticles, the reaction mixture was turned into deep blue polymeric sediment instantaneously. The content was left overnight for the completion of polymerization. The deep blue sediment, i.e., the PANI, was then filtered and washed several times with distilled water. The PANI was dried initially in air followed by vacuum drying for 12 h prior to its further characterizations.

A standard three-electrode setup with two Pt electrodes, one as a working electrode (surface area 0.25 cm^2) and the other as a counter electrode (surface area 1.0 cm^2) and a saturated calomel electrode (SCE) as reference were used for all the electrochemical experiments.

The antibacterial experiments were performed following the standard conventional method by treating the Mn_3O_4 nanoparticle suspension (0.25 g L^{-1}) to various pathogenic organisms at pH 6.2 and 3.3. Bacteria such as *V. cholerae*, *Shigella sp*., *Salmonella sp*., and *E. coli* were grown onto a petri dish. 20 μL of the Mn_3O_4 nanoparticles suspension absorbed on a circular soaking paper was then placed into that dish. The reference antibiotic, ciprofloxacin (20 μL) (obtained from Oxoid, Basingstoke, UK) was also soaked on another similar soaking paper and placed into the same dish. The soaked papers were kept in contact with the bacteria for overnight and the antibacterial activity against the tested bacteria was predicted by measuring the zone diameter of inhibition both by the nanoparticles and the reference antibiotic.

3. Results and discussion

3.1. Synthesis and characterization of Mn_3O_4 nanoparticles

It has already been well addressed that chemical composition, structure and morphology of a material strongly depend on the mode of synthesis employed such as temperature, pH, reaction time, concentration of reactants and products etc. In the present work, attempted was made to prepare Mn_3O_4 nanoparticles from the aqueous solution of $Mn(OOCCH_3)_2$ at 80 °C varying the heating time from 2 to 12 h. In all the syntheses at different heating times, though a well disperse Mn_3O_4 particulates could be observed in the reaction media, the heating time seems to have significant influence on the aggregation of the particulates grown in the media. Fig. 1 shows the SEM micrographs of the Mn_3O_4 powder particles prepared by varying the heating time at 80 °C. It can be seen from the SEM images that Mn_3O_4 has grown with granular morphology in all the three synthesis cases investigated. The result also shows that aggregation of the Mn_3O_4 grains increase with the

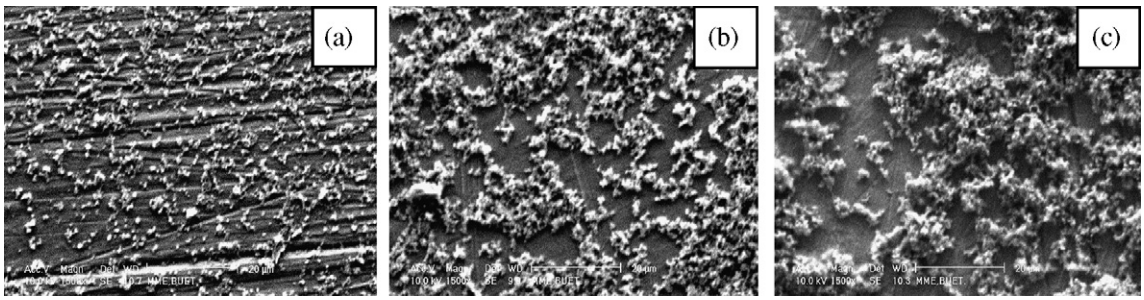

Fig. 1. SEM micrographs of the powder Mn_3O_4 prepared by heating 0.4 M aqueous manganese acetate solution at 80 °C for (a) 2 h, (b) 6 h and (c) 12 h.

increase of heating time. Aggregation of the Mn_3O_4 nanoparticles was also observed in the cases where higher synthesis temperature and higher $Mn(OOCCH_3)_2$ concentration were employed [30]. In order to conduct study with less aggregated samples, we then dealt further in the present work only with the Mn_3O_4 nanoparticles prepared by heating 0.4 M aqueous Mn acetate solution at 80 °C for 2 h.

Elemental analysis of the powder nanoparticles was achieved from the EDX spectra as presented in Fig. 2. The lines observed at 5.90 and 0.64 keV are associated for K and L lines of the Mn element, respectively; the line at 0.52 keV is for K line of the oxygen element and at 2.12 is for M lines of the gold element (that employed as reference substrate). The lines assigned to O and Mn (Fig. 2) agree with those found in a previous report [31]. The average quantities of Mn and O in the prepared Mn_3O_4, according to the EDX spectrum (Fig. 2), are 71.8% and 28.2% respectively.

FT-IR spectral analysis also provided useful qualitative information on the identification of the Mn_3O_4 compounds. The FT-IR spectrum of the present powder nanoparticles displayed three main bands at *ca.* 632.6, 528.5 and 405.0 cm^{-1} which are in agreement with the previous IR findings on Mn_3O_4 compounds [11,32] suggesting that the bands at *ca.* 632.6 and 528.5 are associated with the coupling modes between the Mn–O stretching modes of tetrahedral and octahedral sites and the band at *ca.* 405.0 cm^{-1} is due to the band stretching mode of the octahedral sites. Thus, the result further confirms that the nanoparticles analyzed is Mn_3O_4.

Fig. 3 shows the XRD pattern of the powder Mn_3O_4 nanoparticles. All diffraction peaks can be perfectly indexed to the tetragonal hausmannite structure [33] (space group: I41/amd) with strong ring patterns due to (1 0 1), (1 0 3), (2 1 1), (2 2 0), (2 2 4), and (4 0 0) planes. The Mn_3O_4 lattice constants obtained by refinement of the XRD data of the nanoparticles are $a = b = 5.7630$ Å and $c = 9.4560$ Å, which are consistent with standard values for bulk Mn_3O_4 [33], although the peaks were widened as a result of the small-size effects of the nanoparticles. No characteristic peaks of impurities, such as other forms of manganese oxides, were detected.

Crystallite size was calculated by fitting the synchrotron XRD results using the Scherrer equation, $d = 0.941\gamma/(B\cos\theta_B)$, where γ is the wavelength, B is the full width at half-maximum (FWHM) of the peak, and θ_B is the Bragg angle. The crystallite sizes measured from the four peaks (1 1 2), (1 0 3), (2 1 1), and (224) were averaged to obtain the Mn_3O_4 crystallite size to be *ca.* 10 nm which is in agreement with the TEM observation of the Mn_3O_4 nanoparticles prepared by force hydrolysis of $Mn(OOCCH_3)_2$ solution at 80 °C for 2 h [30].

3.2. Polymerization of aniline by Mn_3O_4 nanoparticles

Aniline can be oxidized to yield PANI, one of the most technologically important material, both by chemical and electrochemical methods. Chemical method is of particular interest since this method is the most feasible route for the production of PANI on a large scale. Chemical polymerization requires an efficient oxidant to oxidize the monomers and also to obtain the polymer with desired properties. Chemical oxidative polymerization of aniline using the oxidants, *viz.* $(NH_4)_2S_2O_8$, $K_2Cr_2O_7$, KIO_3, $FeCl_3$, $KMnO_4$, $KBrO_3$, $KClO_3$, etc. are well addressed [34]. In this study, we attempted chemical oxidative polymerization of aniline using Mn_3O_4 as an oxidant. On addition of Mn_3O_4 nanoparticles suspension to a solution containing H_2SO_4 and aniline, deep blue sediment was found to be formed instantaneously in the reaction mixture. The deep blue sediment thus formed was analyzed to be PANI. The IR spectra of the PANI synthesized using Mn_3O_4 showed principal absorptions at 3460, 3390, 3020, 1590, 1490, 1290 and

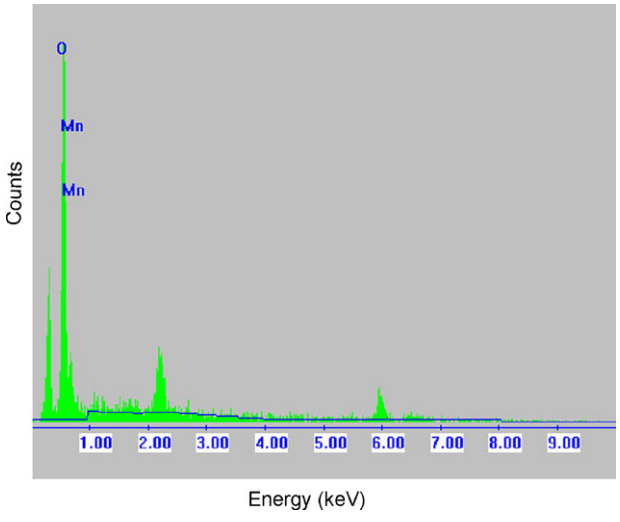

Fig. 2. EDX analysis of the powder Mn_3O_4 nanoparticles prepared by heating 0.4 M aqueous manganese acetate solution at 80 °C for 2 h.

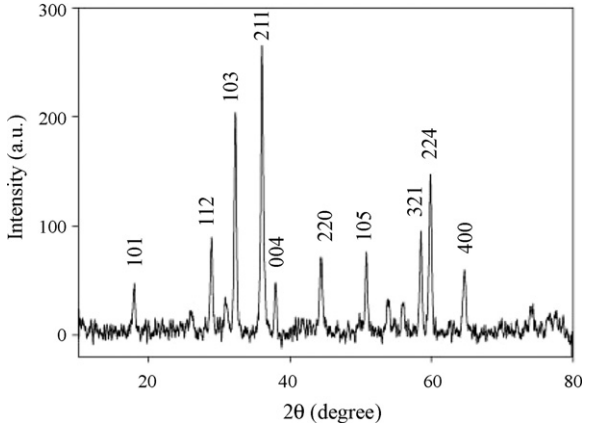

Fig. 3. XRD pattern of Mn_3O_4 nanoparticles prepared as that of Fig. 2.

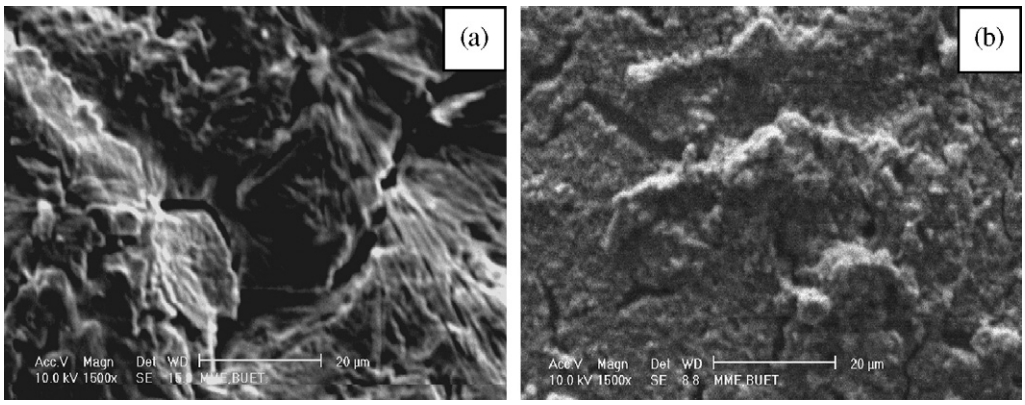

Fig. 4. SEM micrograph of PANI prepared by using (a) Mn_3O_4 nanoparticles and (b) $(NH_4)_2S_2O_8$ oxidant.

830 cm^{-1}, which agreed with that of the PANI synthesized with $(NH_4)_2S_2O_8$ suggesting that the present PANI synthesized using Mn_3O_4 is as emeraldine [35]. The UV–vis absorption spectrum of the present PANI sample (dissolved in NMP under ultrasonic irradiation) showed the characteristic peak *ca.* 307 nm. The absorbance maxima at 307 nm are ascribed to the π–π^* transition within the benzenoid segment [36]. However, a weak shoulder at *ca.* 663 nm was also observed in the present case; this band usually corresponds n–π^* transitions within the quinoid structure. The wavelength of the quinoid band plays an important role in switching PANI from an electric insulator to a conductor upon doping. However, in the present case, PANI was washed several times carefully with distilled water and thus expected to be transformed in its undopped state after washing. Compressed pellet direct-current (dc) electrical conductivity of the solid samples was measured at room temperature by a standard two-point probe method with an autoranging digital multimeter (Keithley 197A, Cleveland, OH, USA). The conductivity of the PANI was measured to be 2.59×10^{-6} S cm^{-1} which seems to be *ca.* five times higher than that of a PANI sample in its neutral or undopped state [37].

Fig. 4 shows the SEM images of PANI prepared by using Mn_3O_4 nanoparticles (a) and $(NH_4)_2S_2O_8$ oxidant (b), respectively. It can be seen from the images that, both the PANI thus obtained with the conventional $(NH_4)_2S_2O_8$ oxidant and Mn_3O_4 nanoparticles, have the uniform compact structures. However, the surface morphology of (b) seems to be a continuous spongy aggregation of grains while in (a) the morphology looks to have the tightest structure like hard-lump or rock-like material. When the morphology and conductivity of the PANI samples (a and b of Fig. 4) are compared, it can be seen that, (a) has higher conductivity and notably different morphological structure than (b). The influence of morphology on electrical conductivity has previously been demonstrated [38]. Thus, the higher electrical conductivity of the present PANI prepared by Mn_3O_4 nanoparticles could be due to the influence of its dissimilar morphological structure.

3.3. Decolorization of dyes by Mn_3O_4 nanoparticles

Oxidizing capacity of the present Mn_3O_4 nanoparticles is further evidenced in the decolorization of dye. Decolorization of the two organic dyes, *viz.*, MB and PR was examined. The performance of Mn_3O_4 nanoparticles on the decolorization of MB dye was investigated spectroscopically. Fig. 5 shows the UV–visible (UV–vis) spectra of the 30 μM MB solution before (a) and after (b–k) charging Mn_3O_4 nanoparticle suspension (0.25 g L^{-1}) at pH 3. Spectrum (a) clearly exhibits the characteristic peaks of MB at *ca.* 614 and 664 nm which are in good agreement to that reported previously [39]. As soon as Mn_3O_4 was added in the dye solution at pH 3, the blue color of the reaction mixture turned to initially light violet and colorless finally. Within a minute after charging the nanoparticle suspension, the characteristic MB peaks plummeted sharply (spectrum-b) showing *ca.* 75% decolorization of the dye. With the further elapse of time, these peaks seem to be disappearing gradually (spectra c–k). Moreover, the original absorption maximum at 664 nm is shifted to 618, 615, 612 and 610 nm after 1, 3, 5 and 7 min, respectively. Within 30 min, this absorption band became so broad that no obvious band could be traced suggesting nearly complete decolorization of MB. Inset shows the camera photographs of 30 μM MB solution taken before (x) and at 24 h after (y) charging Mn_3O_4 nanoparticle suspension (0.25 g L^{-1}) at pH 3. Decolorization of PR was also achieved by the Mn_3O_4 nanoparticles. The results are shown in Fig. 6. It can be seen from the results that the Mn_3O_4 could decolorize PR almost completely with in 24 h. The inset shows the photographs of 200 μM PR solution taken before (m) and at 24 h after (n) charging Mn_3O_4 nanoparticle suspension (0.25 g L^{-1}) at pH 3. Decolorization of a real sample, i.e., dye effluent of a local textile industry, was also attempted by using Mn_3O_4 nanoparticle

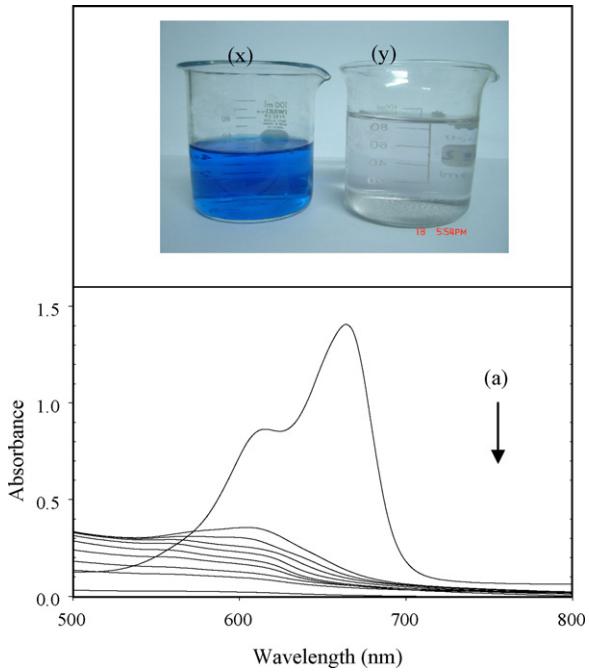

Fig. 5. UV–vis spectra of 30 μM MB dye solution before (a) and after (b–k) charging the Mn_3O_4 nanoparticles at pH 3. The spectra taken at different time intervals, *viz.*, 1, 3, 5, 7, 10, 15, 20, 30, 60 min and 24 h after charging the nanoparticles correspond the spectra (b–k), respectively. Inset shows camera pictures of 30 μM MB dye solution before (x) and after (y) charging the Mn_3O_4 nanoparticles.

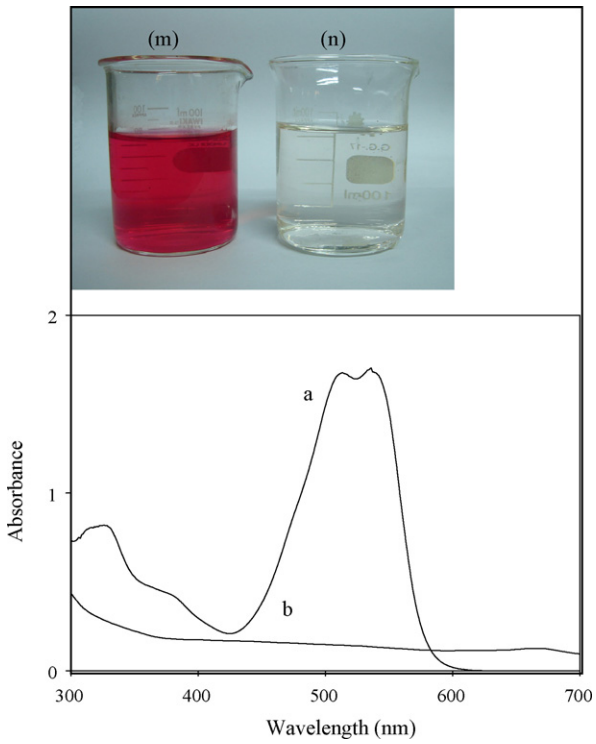

Fig. 6. UV–vis spectra of 300 μM PR dye solution before (a) and at 24 h after (b) charging the Mn_3O_4 nanoparticles at pH 3. Inset shows the camera pictures of 300 μM PR dye solution before (m) and after (n) charging the Mn_3O_4 nanoparticles.

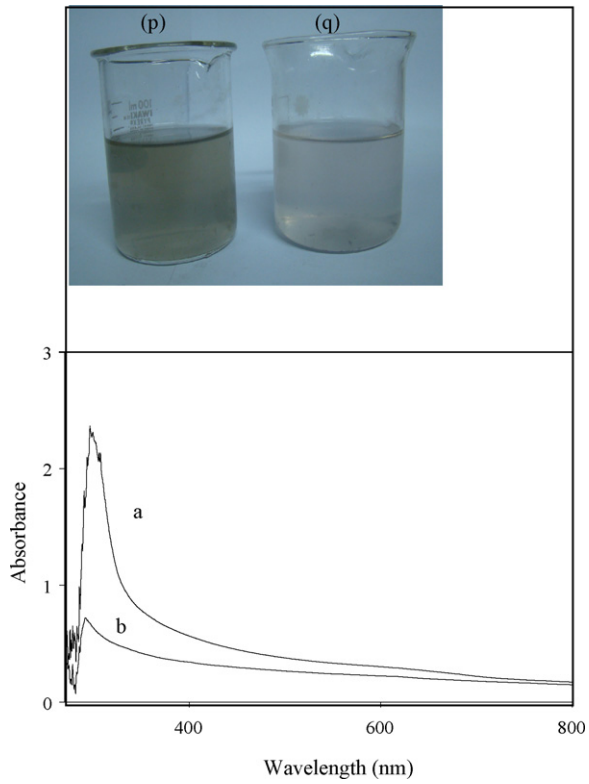

Fig. 7. UV–vis spectra of the textile dye effluent before (a) and at 24 h after (b) charging the Mn_3O_4 nanoparticles at pH 3. Inset shows the camera pictures of the dye effluent before (p) and after (q) charging the Mn_3O_4 nanoparticles.

suspension (0.25 g L^{-1}) at pH 3. Alike MB and PR, the dye effluent was also found to be decolorized successfully by treating with Mn_3O_4. Fig. 7 shows the UV–vis spectral changes of the dye effluent before and after charging the nanoparticle. The strong band at *ca*. 310 nm of the effluent reduced to more than 70% on charging the nanoparticles suggesting the decolorization of the dye from the effluent. Inset shows the camera pictures of the dye effluent before and after decolorization.

Decolorization of MB was investigated further by electrochemical means. Fig. 8 shows the cyclic voltammograms (CVs) of the MB dye solution in H_2SO_4 solution between the potential −0.2 and +0.5 V at a scan rate of 100 mV s^{-1}. The CV (a) clearly shows that the MB solution can be switched between its oxidized and reduced states; the CV is composed of a well-defined redox process showing the anodic process at *ca.* +0.26 V and the cathodic one at *ca.* 0.21 V, suggesting the oxidation and reduction of MB, respectively [40]. However, this redox process of the MB seems to be diminished or became very weak, as can be seen from the CV (b), when the MB solution was treated with Mn_3O_4 nanoparticles for 24 h. From the electrochemical measurement, it seems to be evident again that decolorization of the MB dye can be achieved on treating the dye with Mn_3O_4 nanoparticles.

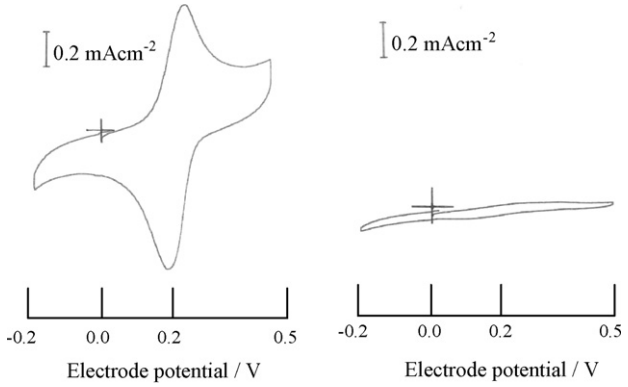

Fig. 8. CV of 30 μM MB in 0.25 M H_2SO_4 solution (a) before decolorization and (b) after decolorization for 24 h with 0.25 g L^{-1} Mn_3O_4 nanoparticles suspension.

Influence of medium pH on the decolorization of MB dye was also investigated. Fig. 9 shows the decolorization of 30 μM MB at (a) pH 3 and (b) pH 5 using the Mn_3O_4 nanoparticles suspension. It can be seen from the result that both the degree and rate of MB decolorization are enhanced at lower pH medium. It is also to be noted here that at pH 7 there was hardly any decolorization of MB. Thus, it appears that the role of acid in the present decolorization process is indeed indispensable.

It has been well established that oxidative degradation of organic matter by Mn oxides is via a surface mechanism [41], that is, the organic compound is adsorbed on surface of Mn oxides to form a surface precursor complex, electron transfer then occurs within the surface complex from organic reductant to the surface-

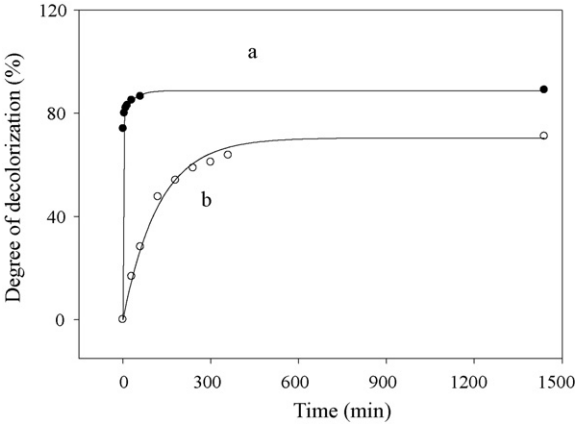

Fig. 9. Effect of medium pH on the MB dye (30 μM) decolorization using Mn_3O_4 nanoparticles (0.25 g L^{-1}).

Table 2
Antibacterial activity of the Mn_3O_4 nanoparticles suspension (0.25 g L^{-1}) against different pathogenic organisms.

Bacteria	Zone diameter of inhibition (mm)			
	pH = 6.2		pH = 3.3	
	Mn_3O_4 suspension	Control (ciprofloxacin)	Mn_3O_4 suspension	Control (ciprofloxacin)
Vibrio cholerae	S*16	S*33	S*16	S*30
Shigella sp.	S*14	S*26	S*14	S*30
Salmonella sp.	S*15	S*20	S*13	S*22
Escherichia coli	R*	S*32	S*12	S*30

S* and R* stand for sensitive and resistant, respectively.

bound Mn(III, IV), followed by release of organic oxidation products and Mn(II) arising from reductive dissolution of Mn oxides. In the present study, decolorization of the dyes by the Mn_3O_4 nanoparticle is most likely to follow this surface mechanism, as do many other organic pollutants [15–17] including MB dye [42].

3.4. Antibacterial activity of Mn_3O_4 nanoparticles

The antibacterial activity of Mn_3O_4 nanoparticles (0.25 g L^{-1}) at pH 6.2 and 3.3 against various pathogenic organisms was tested. The results are presented in Table 2. The bacteria tested are *V. cholerae* causing cholera, *Shigella sp*. causing dysentery, *Salmonella sp*. causing diarrhea and enteric fever like typhoid and *E. coli* causing diarrhea. In order to assess the antibacterial activity, zone diameter of inhibition observed by both the Mn_3O_4 and the control ciprofloxacin antibiotic were measured. It can be seen from the result given in Table 2 that the activity of Mn_3O_4 against the bacterial growth is *ca*. half than that of the control ciprofloxacin antibiotic suggesting a moderate antibacterial activity against the bacteria samples tested. Whatever the mechanism may be, this result implies that Mn_3O_4 nanoparticles can kill some bacteria and interacts with them relatively strongly at pH 3.3 than pH 6.2. However, no detectable antibacterial activity can be achieved once the concentration of the Mn_3O_4 nanoparticles in the suspension is lowered to the order of 10^{-2}.

4. Conclusion

Mn_3O_4 nanoparticle, prepared by forced hydrolysis method, is a promising material for decolorization of MB and PR dyes from water. Decolorization of the dyes is believed to be occurred through oxidative degradation via a surface mechanism. pH of the decolorization medium exerts significant effect on the degree of dye decolorization. At lower pH, the Mn_3O_4 nanoparticles show superior capacity of decolorization; the degree of decolorization of MB by Mn_3O_4 nanoparticles reached more than 75% within 1 min at the pH as low as 3. The promising oxidative capacity of the Mn_3O_4 nanoparticles was further demonstrated in the polymerization reaction of aniline monomer. The PANI thus formed by using Mn_3O_4 nanoparticle is emeraldine in nature and possess the characteristic properties as that of PANI prepared by the well known $(NH_4)_2S_2O_8$ oxidant. In addition to oxidative capacity, Mn_3O_4 nanoparticles also show moderate antibacterial activity against the bacteria *V. cholerae*, *Shigella sp*., *Salmonella sp*., and *E. coli.* which are responsible for cholera, dysentery, typhoid, and diarrhea diseases, respectively. Antibacterial activity of the Mn_3O_4 nanoparticle is nearly half to that of the standard ciprofloxacin antibiotic that effectively used for the prevention of the above mentioned diseases worldwide.

References

[1] Y.F. Shen, R.P. Zerger, R.N. DeGuzman, S.L. Suib, L. McCurdy, D.I. Potter, C.L. O'Young, Manganese oxide octahedral molecular sieves: preparation, characterization, and applications, Science 260 (1993) 511–515.
[2] F. Qi, H. Karoh, K. Ooi, M. Tani, Y. Nakacho, Synthesis of hollandite-type manganese-dioxide with H^+ form for lithium rechargeable battery, J. Electrochem. Soc. 141 (1994) L135–L136.
[3] A.R. Armstrong, P.G. Bruce, Synthesis of layered $LiMnO_2$ as an electrode for rechargeable lithium batteries, Nature 381 (1996) 499–500.
[4] S.I.C. de Torresi, A. Gorenstein, Electrochromic behaviour of manganese dioxide electrodes in slightly alkaline solutions, Electrochim. Acta 37 (1992) 2015–2019.
[5] E.R. Stobhe, B.A.D. Boer, J.W. Geus, The reduction and oxidation behaviour of manganese oxides, Catal. Today 47 (1999) 161–167.
[6] E.J. Grootendorst, Y. Verbeek, V. Ponec, The role of the Mars and Van Krevelen mechanism in the selective oxidation of nitrosobenzene and the deoxygenation of nitrobenzene on oxidic catalysts, J. Catal. 157 (1995) 706–712.
[7] M. Baldi, E. Finocchio, F. Milella, G. Busca, Catalytic combustion of C3 hydrocarbons and oxygenates over Mn_3O_4, Appl. Catal. B: Environ. 16 (1998) 43–51.
[8] M.M. Zwinkels, S.G. Jaras, P.G. Menon, T.A. Griffin, Catalytic materials for high temperature combustion, Catal. Rev. Sci. Eng. 35 (1993) 319–358.
[9] A. Manceau, V.A. Drits, E. Silvester, C. Bartoli, B. Lanson, Structural mechanism of Co^{2+} oxidation by the phyllomanganate buserite, Am. Miner. 82 (1997) 1150–1175.
[10] J.G. Kim, J.B. Dixon, C.C. Chusuei, Y. Deng, Oxidation of chromium(III) to (VI) by manganese oxides, Soil Sci. Soc. Am. J. 66 (2002) 306–315.
[11] V.Q. Chiu, J.G. Hering, Arsenic adsorption and oxidation at manganite surfaces. 1. Method for simultaneous determination of adsorbed and dissolved arsenic species, Environ. Sci. Technol. 34 (2000) 2029–2034.
[12] N. Belzile, Y.-W. Chen, Z. Wang, Oxidation of antimony(III) by amorphous iron and manganese oxyhydroxides, Chem. Geol. 174 (2001) 379–387.
[13] M.J. Scott, J.J. Morgan, Reactions at oxide surfaces. 2. Oxidation of Se(IV) by synthetic birnessite, Environ. Sci. Technol. 30 (1996) 1990–1996.
[14] C.J. Matocha, D.L. Sparks, J.E. Amonette, R.K. Kukkadapu, Kinetics and mechanism of birnessite reduction by catechol, Soil Sci. Soc. Am. J. 65 (2001) 58–66.
[15] R.A. Petrie, P.R. Grossl, R.C. Sims, Oxidation of pentachlorophenol in manganese oxide suspensions under controlled Eh and pH environments, Environ. Sci. Technol. 36 (2002) 3744–3748.
[16] H. Li, L.S. Lee, D.G. Schulze, C. Guest, Role of soil manganese in the oxidation of aromatic amines, Environ. Sci. Technol. 37 (2003) 2686–2693.
[17] H. Zhang, C.-H. Huang, Oxidative transformation of fluoroquinolone antibacterial agents and structurally related amines by manganese oxide, Environ. Sci. Technol. 39 (2005) 4474–4483.
[18] K.-H. Kang, D.-M. Lim, H. Shin, Oxidative-coupling reaction of TNT reduction products by manganese oxide, Water Res. 40 (2006) 903–910.
[19] K.R. Reddy, R.D. DeLaune, Biogeochemistry of Wetlands: Science and Applications, CRC Press, New York, NY, USA, 2008.
[20] P. Grau, Textile industry wastewater treatment, Water Sci. Technol. 24 (1) (1991) 97–103.
[21] Y.M. Sloker, A.M. Le Marechal, Methods of decolorization of textile wastewater, Dyes Pigments 37 (1998) 335–356.
[22] M.A. Brown, S.C. De Vito, Predicting azo dye toxicity, Crit. Rev. Environ. Sci. Technol. 23 (1993) 249–324.
[23] Y. Al-Degs, M.A. Khraisheh, M.F. Tutunji, Sorption of lead ions on diatomite and manganese oxides modified diatomite, Water Res. 35 (2001) 3724–3728.
[24] H.-J. Fan, P.R. Anderson, Copper and cadmium removal by Mn oxide coated granular activated carbon, Sep. Purif. Technol. 45 (2005) 61–67.
[25] J. de Ruddera, T.V. de Wielea, W. Dhoogeb, F. Comhaireb, W. Verstraetea, Advanced water treatment with manganese oxide for the removal of 17α-ethynylestradiol (EE2), Water Res. 38 (2004) 184–192.
[26] G.M. Hettiarachchi, G.M. Pierzynski, M.D. Ransom, In situ stabilization of soil lead using phosphorus and manganese oxide, Environ. Sci. Technol. 34 (2000) 4614–4619.
[27] J. Ge, J. Qu, Degradation of azo dye acid red B on manganese dioxide in the absence and presence of ultrasonic irradiation, J. Hazard. Mater. 100 (2003) 197–207.
[28] R. Liu, H. Tang, Oxidative decolorization of direct light red F3B dye at natural manganese mineral surface, Water Res. 34 (2000) 4029–4035.
[29] E. Deschamps, V.S.T. Ciminelli, W.H. H¨oll, Removal of As(III) and As(V) from water using a natural Fe and Mn enriched sample, Water Res. 39 (2005) 5212–5220.
[30] M. Ocana, Uniform particles of manganese compounds obtained by forced hydrolysis of manganese(II) acetate, Colloid Polym. Sci 278 (2000) 443–449.

[31] A.J. Nelsona, J.G. Reynoldsa, J.W. Roosb, Comprehensive characterization of engine deposits from fuel containing MMT, Sci. Total Environ. 295 (2002) 183–205.
[32] A.K.H. Nohman, M.I. Zaki, S.A.A. Mansour, R.B. Fahim, C. Kappenstein, Characterization of the thermal genesis course of manganese oxides from inorganic precursors, Thermochim. Acta 210 (1992) 103–121.
[33] International Centre for Diffraction Data (ICDD), PDF file no. 24-0734.
[34] Y. Cao, A. Andretta, A.J. Heeger, P. Smith, Influence of chemical polymerization conditions on the properties of polyaniline, Polymer 30 (1989) 2305–2311.
[35] A.P. Monkman, P. Adams, Optical and electronic properties of stretch-oriented solution-cast polyaniline films, Synth. Met. 40 (1991) 87.
[36] F. Wudl, R.O. Angus Jr., F.L. Lu, P.M. Allemand, D. Vachon, M. Nowak, Z.X. Liu, H. Schaffer, A.J. Heeger, Poly-p-phenyleneamineimine: synthesis and comparison to polyaniline, J. Am. Chem. Soc. 109 (1987) 3384–3677.
[37] P.M. McManus, S.C. Yang, R.J. Cushman, Electrochemical doping of polyaniline: effects on conductivity and optical spectra, J. Chem. Soc., Chem. Commun. 22 (1985) 1556–1557.
[38] A. Gok, M. Omastova, A.G. Yavuz, Synthesis and characterization of polythiophenes prepared in the presence of surfactants, Synth. Met. 157 (2007) 23–29.
[39] T.Y. Zhang, T. Oyama, A. Aoshima, H. Hidaka, J.C. Zhao, N. Serpone, Photooxidative *N*-demethylation of methylene blue in aqueous TiO_2 dispersions under UV irradiation, J. Photochem. Photobiol. A 140 (2001) 163–172.
[40] V. Svetliic, J. Clavilier, V. Zutic, J. Chevalet, Electrochemical evidence of two-dimensional surface compounds of heterocyclic molecules at sulphur-covered gold and platinum. Part I. Methylene blue, J. Electroanal. Chem. 312 (1991) 205–218.
[41] A.T. Stone, J.J. Morgan, Reduction and dissolution of manganese(III) and manganese(IV) oxides by organics. 1. Reaction with hydroquinone, Environ. Sci. Technol. 18 (1984) 450–456.
[42] M.-X. Zhu, Z. Wang, L.-Y. Zhou, Oxidative decolorization of methylene blue using pelagite, J. Hazard. Mater. 150 (2008) 37–45.